45th AIAA Aerospace Sciences Meeting and Exhibit

Turbine Blade Tip Leakage Flow Control: Thick/Thin Blade Effects

Julia Stephens* , Thomas Corke† and Scott Morris‡

Center for Flow Physics and Control (FlowPAC), University of Notre Dame, Notre Dame, IN 46556

An experiment was conducted in a linear cascade of Pak-B blades for an exit Mach number of 0.3 to simulate the flow in the tip-gap region of a low pressure turbine blade row. The experiment focused on the independent effects of thickness-to-gap and gap-to-chord ratios on the tip-gap flow behavior. Two extreme gap-to-chord ratios of 5% and 8% were chosen, for which four thickness-to-gap ratios were examined. The flow was documented through blade-tip and end-wall static pressure measurements, and downstream total pressure loss coefficients. Additionally, surface flow visualization was performed on the blade tip end for a greater understanding of the gap-flow behavior. The response of the flow to passive flow control using a partial suction-side squealer tip at each of the thickness-to-gap and gap-to-chord cases was documented. The intention was to examine any sensitivity of the flow to the gap-to-chord ratio that might be attributed to the thickness-to-gap ratio in a manner that can be categorized as "thick" and "thin" blade behavior. For this the focus was on possible changes in the size and location of a separation and re-attachment lines on the blade tip end. Defining such features in these flows is important to our goal of active tip-gap flow control using plasma actuators because they are highly receptivity to unsteady forcing.

I. Introduction

It is desirable to further increase the efficiency of turbomachines. As an example of the impact this can have, it is estimated[1] that just a 1% improvement in the efficiency of commercial aircraft engines would save over $200M per year. As a result, the study of where losses in efficiency occur and how to reduce them is of prime interest.

One area of loss in a gas turbine engine is due to the over-the-tip leakage flow in the turbine stage. This is a result of the fluid leakage through the gap between the blade and the casing wall. Besides the obvious effect of altering the blade loading near the tip, the leakage flow results in the formation of three-dimensional vortical structures that produce irreversible losses in work. The behavior of this flow both in the gap, and as it interacts with other flow structures downstream, has been studied extensively.[2–10] The interaction between the tip vortex and the passage vortex, caused by overturning of the end-wall boundary layer fluid, is of particular interest.

It is known that smaller gaps result in lower rotor losses. In fact, removing the gap altogether would be ideal. Virtual gap removal through wall treatments is an ongoing area of research. On-blade treatments such as squealer tips have been employed and shown to be effective in increasing the blockage in the gap with less risk of catastrophic failure due to rub.[11–13] A downside of this approach is that it sets up secondary flow motions under the tip that enhance heat transfer that can quickly erode the blade tip.

Heyes[14] investigated various forms of squealers and determined that a partial suction-side squealer was sufficient to produce the effects of a full squealer cavity. In addition to squealers, Booth[11] proposed using a pressure-side winglet to affect the flow over the tip. Squealer-winglet combinations have also been explored. Papa[13] found that the best combination was a pressure-side winglet with a suction-side squealer.

*Graduate Research Assistant, AIAA Student Member.
†Clark Chair Professor, Associate Fellow AIAA.
‡Assistant Professor, Member AIAA

In previous studies of passive flow control using a partial suction-side squealer tip,[15] the tip flow became less sensitive to a squealer tip when the blade thickness-to-gap ratio was less than 4. Denton[7] proposed that the behavior of the flow in the gap changes with the thickness-to-gap ratio. He found that if the blade thickness is more than about four times the gap size, the flow behaves as a "thick" blade. The flow topology of a "thick" blade consisted of a a separation and re-attachment line that formed on the blade tip.

If the blade were "thin" according to Denton,[7] the flow separates from the pressure-side blade edge and never re-attaches on the blase tip. Figure 1 depicts the flow topology of "thick" and "thin" blades. Douville et al.[15] proposed a slightly different threshold between "thick-thin" behavour that was at a $g/c = 3.5$.

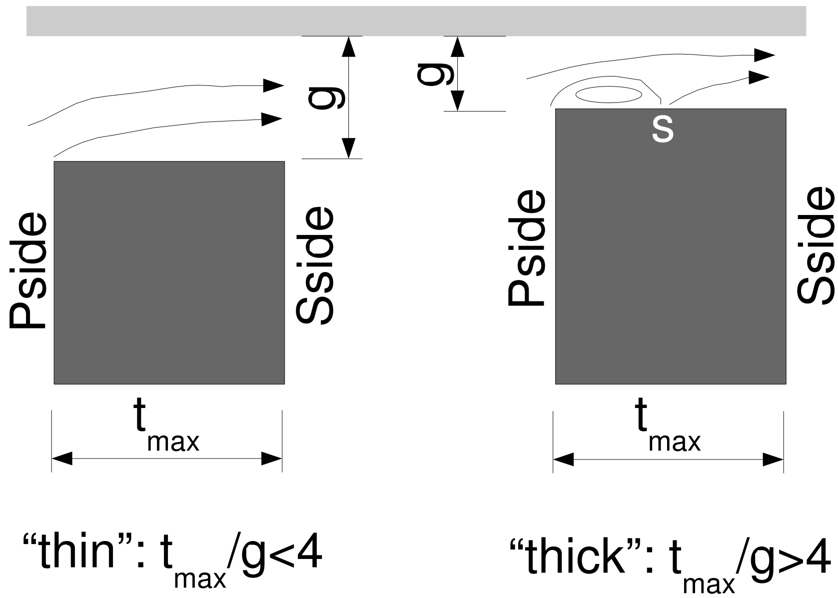

Figure 1. Schematic of flow topology that distinguishes between "thick" and "thin" blades.

The object of this work was to study the independent effects of thickness-to-gap and gap-to-chord ratios on the flow topology associated with "thick" and "thin" blades. This involved two extreme gap-to-chord ratios of 5% and 8%, and four thickness-to-gap ratios. The differences in the flow resulting from these conditions were documented by blade-tip and end-wall static pressure measurements, as well as downstream total pressure loss coefficients. Additionally, flow visualization was performed on the blade tip end to document flow separation and re-attachment characteristics. The response of the flow to passive flow control using a partial suction side squealer at each of the thickness-to-gap and gap-to-chord cases was then documented. The sensitivity of the flow to combinations of thickness-to-gap and gap-to-chord ratios with respect to the published "thick" and "thin" blade categories was then summarized. These results are then put in context with a change in the size and location of a separation and re-attachment line on the blade tip end. Defining the location of separation and reattachment lines is important to our goal of active tip-gap flow control using plasma actuators because such flow features are traditionally highly receptive to unsteady forcing. The ultimate intention is to affect the tip-vortex formation and downstream mixing by exciting an instability of the blade-gap flow by unsteady forcing through a plasma actuator located on the blade tip.

II. Experimental Setup

This research was performed in a transonic linear cascade in the Hessert Laboratory at the University of Notre Dame. A schematic and photograph of the facility are shown in Figure 2. All of the cases in this study were performed at an inlet Reynolds number of 0.5×10^6, corresponding to an inlet Mach number of 0.2 and an exit Mach number of 0.3. The setup was a three blade (2 passage) linear cascade comprised of a Pratt & Whitney Pak-B low pressure turbine blade shape. The stagger angle of the blades was 26.16 degrees. The blades had a chord, c of 4.61 inches, an axial chord, c_x of 4.14 inches, a span of 4 inches, and a solidity, σ of 1.13. The outer two blades spanned the entire cascade and intersected the tunnel walls at both spanwise locations. The middle blade was instrumented and cantilevered from the inside wall leaving a small tip clearance from the outside end-wall. Removable plastic shim spacers shaped like the blade profile were added to the center blade to provide different gap spacings. The shims permitted gap sizes of up to 8.0% c_x.

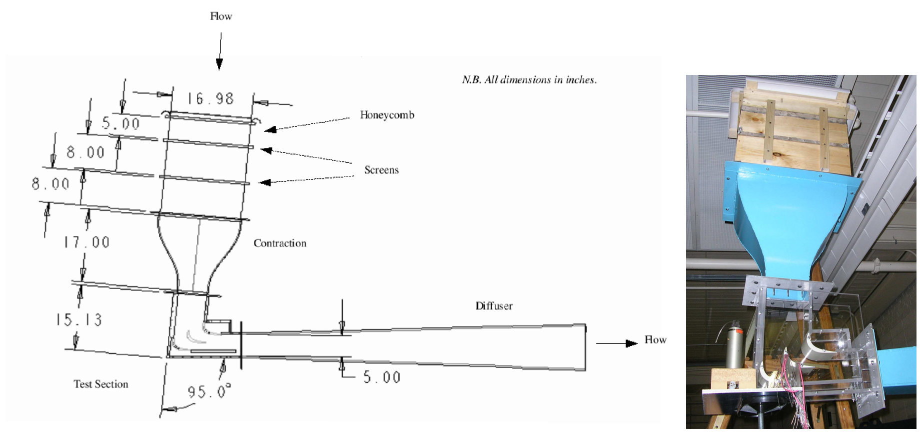

(a) Wind Tunnel (b) Test Section

Figure 2. Schematic drawing of Transonic Linear Cascade Facility and a corresponding photograph of the facility. Note all dimensions are in inches.

All three of the blades in the cascade were cast in a two-part epoxy from a numerically machined mold. The center blade was divided into three parts: a main molded blade with a span of 3.42 in., a removable molded blade segment with a span of 0.1875 in., and removable blade tip winglets made of glass epoxy board with a span of 0.0625 in.

One end of the main blade segment was attached to the back wall of the cascade section. The 0.1875 in. removable segment was attached to the other end of the main blade segment. Spacers with the same blade profile could be placed between the removable blade segment and the main blade to vary the distance between the blade end and the front wall of the cascade section.

The winglets were machined using a numerically controlled milling machine from 0.0625 in. thick glass-epoxy boards that were originally copper-clad on both sides. The copper cladding was also machined off using the same milling machine to leave electrodes that were a part of the plasma actuator when active control was done.

A set of different size winglets were produced. A photograph of these are shown in Figure 3. The winlets used with the 5% gap-to-chord are shown as the left column in the photograph. Those used with the 8% gap-to-chord are shown as the right column. For the 5% gap-to-chord ratio, these gave thickness-to-gap ratios of 2.83, 3.3, 3.7, and 4.3. For the 8% gap-to-chord ratio, these gave thickness-to-gap ratios of 1.75, 2.83, 3.3, and 3.7.

The squealer used in the experiments was a partial, suction-side type. It consisted of a 0.031 in. thick metal strip that was contoured to the shape of the blade profile and bonded to its end. The height of the strip was $\tau = 0.1035$ in. which corresponded to $\tau/c_x = 0.025$. It did not change in height with changes in the thickness-to-gap. The partial squealer extended over the center 75% of the blade profile. It can be seen mounted on the end of a blade in the photograph in Figure 4.

Static pressure taps were located at the end of the main blade portion of the center blade. These provided measurement of the static pressure near the end of the blade. Because they were on the edge of the main blade, their location relative to the end of the built-up blade changed as spacers were added to vary the tip-gap. As an example, for the 8% gap-to-chord case, the pressure taps were $0.06c_x$ from the tip, while for the 5% gap-to-chord case, the pressure taps were $0.09c_x$ from the tip.

Thirty (30) static pressure ports were also located on the end-wall under the blade. The distribution of the wall pressure taps relative to the blade location is shown in Figure 5.

The flowfield in the wake of the center blade was documented using a five-hole Pitot probe that was mounted to a motorized traverse system. The coordinate system for these measurements is shown in Figure 6. The measurements surveyed a 2 in. by 1.25 in. region that was divided into a 10 by 10 point grid. The surveys were performed at a distance of one C_x downstream of the trailing edge of the center blade. They encompassed one third of the blade span from end-wall.

Figure 3. Photograph of winglets used to create various thickness-to-gap ratios on the measurement Pak-B blade. The left set was used with the 5% gap-to-chord setup. The right set was used with the 8% gap-to-chord setup.

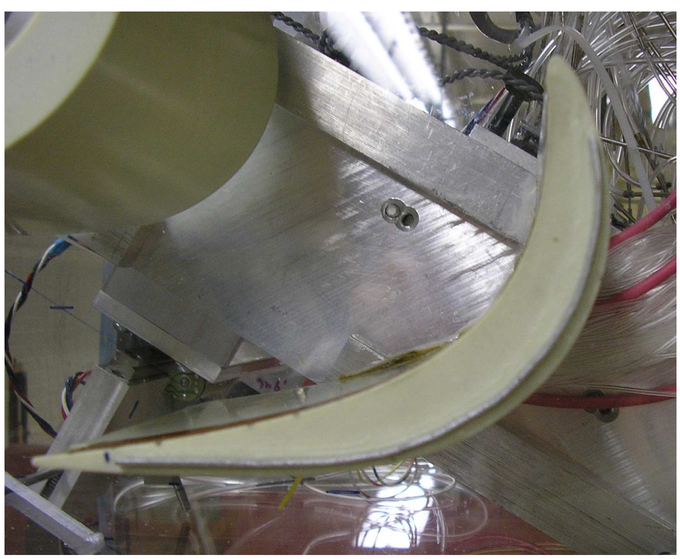

Figure 4. Photograph of Pak-B blade tip showing partial suction-side squealer tip. The squealer tip is the thin strip on the outer edge of the blade end. It is 0.031 in. thick and 0.1035 in.tall.

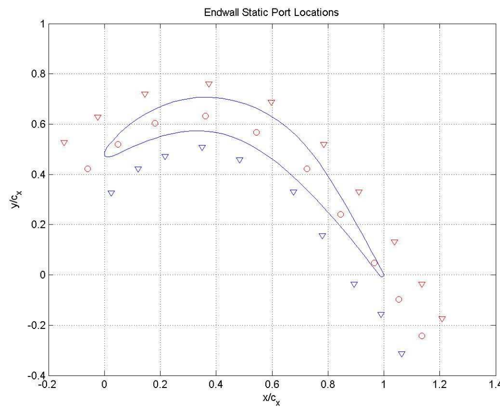

Figure 5. Distribution of the wall pressure taps relative to the blade location.

The method used to evaluate the pressure readings from the five hole probe followed that of Douville et al.[15] This yielded the total pressure and mean velocity vector at each measurement point in the flow. These were used to construct spatial distributions of the total pressure loss, mean velocity field, and vorticity field in the measurement region.

The method of surface flow visualization followed that of Langston[16] and Aunapu.[17] This involved covering the tip of the blade with a white contact paper. An extra-fine point water-proof marker was used to make black dots in a pattern on the paper. An air brush was then used to spray on a thin wet coating of methyl salicylate (also known as oil of winter green) on the paper. The methyl salicylate absorbed the marker ink so that when the tunnel was turned on and brought quickly up to speed, the the ink was transported by the local surface shear stress. When the tunnel was turned off and the methyl salicylate completely evaporated, the ink traces were fixed to the contact paper. The paper was then removed and digitally scanned.

Three surface flow visualization runs were performed for each experimental condition. The images from the runs were then averaged.

III. Results

Contour plots of the total pressure loss in the wake along with the corresponding velocity vectors for all the thickness-to-gaps at a 5% g/c are shown in Figure 7. The flat tip cases are shown as the top row, and the squealer tip cases are shown as the bottom row. Note that the wall is at the right edge of each plot, and the blade-end/wall intersection is at the upper right corner of each plot.

The highest loss coefficients (yellow with red region) are associated with the tip-gap vortex. Both a change in the magnitude and center location of the maximum loss coefficient are observed to occur by changing t/g, with and without the squealer tip. In order to try to quantify the motion of the center of the maximum loss coefficient, its $y-z$ position was defined as $|yz| = ((y/pitch)^2 + (z/span)^2)^{1/2}$. This is presented as a function of the t/g for the 5% g/c in Figure 8.

For the baseline flat tip case, the location of the maximum loss coefficient center changes almost linearly with t/g up to $t/g \simeq 3.5$. This is close to the t/g criteria for "thick" blades given by Douville et al.[15] Beyond that t/g, the location of the maximum loss coefficient center is insensitive to the thickness-to-gap ratio. With the addition of the squealer, the maximum loss coefficient location is closer to the end wall, and its position is less sensitive to the change in the thickness-to-gap ratio.

Contour plots of the total pressure loss in the wake along with the corresponding velocity vectors for all the thickness-to-gaps at a 8% g/c are shown in Figure 9. The flat tip cases are shown as the top row, and the squealer tip cases are shown as the bottom row.

Again the highest loss coefficients (red regions) are associated with the tip-gap vortex. The magnitude and center location of the maximum loss coefficient are again observed to depend on the t/g, and the addition of the squealer tip. The position of the maximum loss coefficient center is presented as a function of the t/g for the 8% g/c in Figure 10.

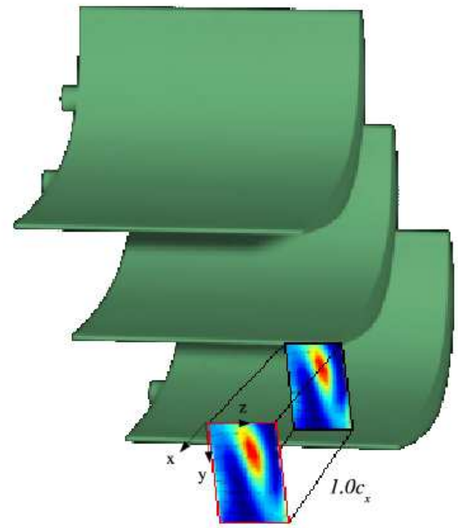

Figure 6. Coordinate system for blade wake surveys made using 5-hole Pitot probe.

For the baseline flat tip case, the location of the maximum loss coefficient center again changed almost linearly with the thickness-to-gap ratio up to $t/g \simeq 3.5$. For $t/g > 3.5$, its location was asymptoting in a manner similar to the 5% g/c case.

With the addition of the squealer, the tip-gap vortex location was closer to the end wall, and its position became less sensitive to the change in the thickness-to-gap ratio at a slightly lower $t/g \simeq 3$.

Pressure distributions at the end of the blade near the tip for the 5% g/c at all of the thickness-to-chord values are plotted in Figure 11. The solid line connecting points corresponds to the pressure distribution at the mid-span of the blade with the tip-gap closed. The dotted curve corresponds to the distribution from an Euler simulation for infinite aspect ratio Pak-B blades. Both of these are shown for reference.

The pressure distributions for the different t/g ratios roughly overlay each other except at the trailing edge on the suction side of the blade. The larger negative C_p values near the trailing edge are indicative of the tip-gap vortex. This appears to be stronger for the smaller thickness-to-gap values. In addition the change with t/g ratio seems to decrease for $t/g > 3.7$, which is the approximate transition from "thin" to "thick" blades.

Integrating the C_p distributions in Figure 11 provides a measure of the blade loading near the tip. The blade loading for the 5% g/c is shown in Figure 12. For the baseline flat-tip case, the blade loading initially decreases with increasing t/g up to $t/g \simeq 3.5$. For $t/g > 3.5$, the blade loading increases slightly then asymptotes.

The addition of the squealer tip increases the tip loading for all of the thickness-to-gap ratios at the 5% g/c. The trend with g/c generally follows that of the baseline case, with a minimum blade loading occurring at the same $t/g \simeq 3.5$.

Pressure distributions at the end of the blade near the tip for the 8% g/c at all of the thickness-to-chord values are plotted in Figure 13. Again for reference, the solid line connecting points corresponds to the pressure distribution at the mid-span of the blade with the tip-gap closed, and the dotted curve corresponds to the distribution from an Euler simulation for infinite aspect ratio Pak-B blades.

Again the pressure distributions for the different t/g ratios are observed to roughly overlay each other except at the trailing edge on the suction side of the blade. The larger negative C_p values near the trailing edge indicate a stronger tip-gap vortex than with the smaller (5%) g/c. Also in contrast to the smaller gap-to-chord case, the strength of the vortex appears to continually increase with increasing t/g.

Integrating C_p distributions in Figure 13 provides a measure of the blade loading near the tip. This is shown in Figure 14. The effect of t/g on the blade loading for the 8% g/c is quite different from the 5% g/c. Although there is a good deal of scatter in the results for the baseline flat-tip case, the general trend is an

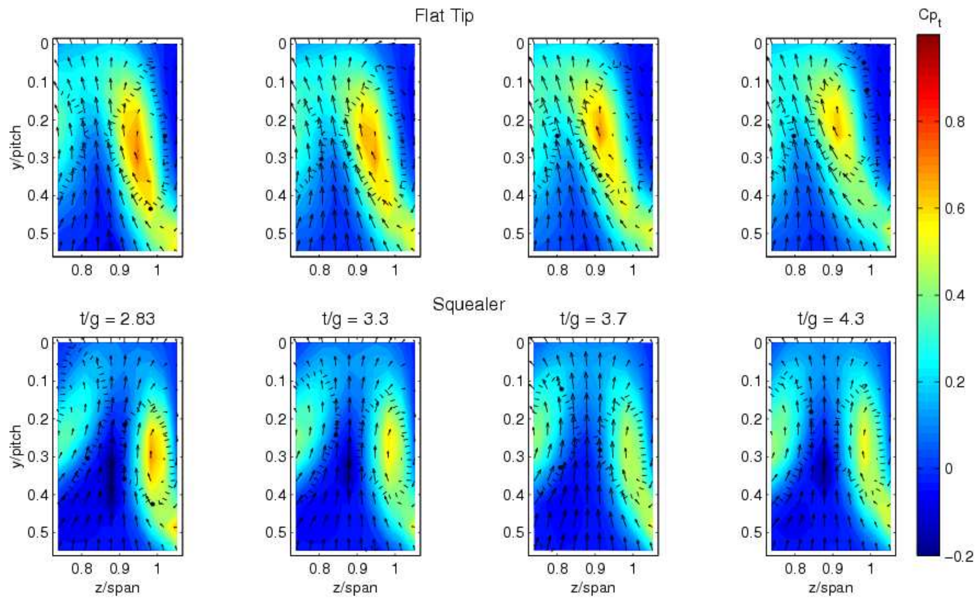

Figure 7. Coefficient of pressure distribution for different winglets producing different thickness-to-gap ratios for a 5% gap to chord ratio.

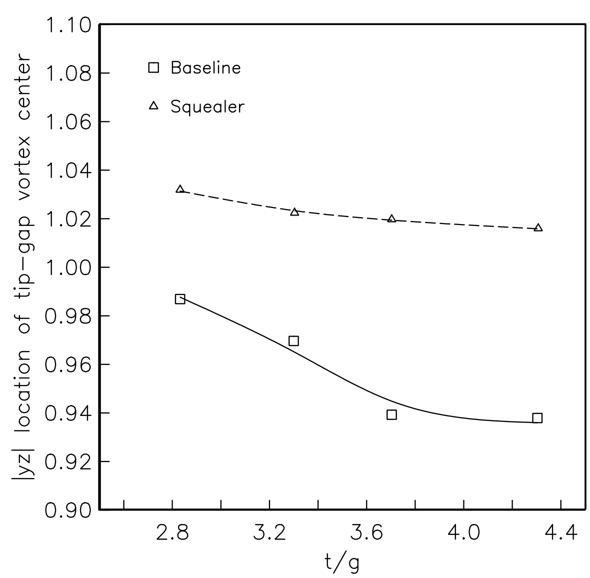

Figure 8. Magnitudes of the locations of the center of the tip-gap vortex as a function of the thickness-to-gap ratio at a 5% gap-to-chord ratio.

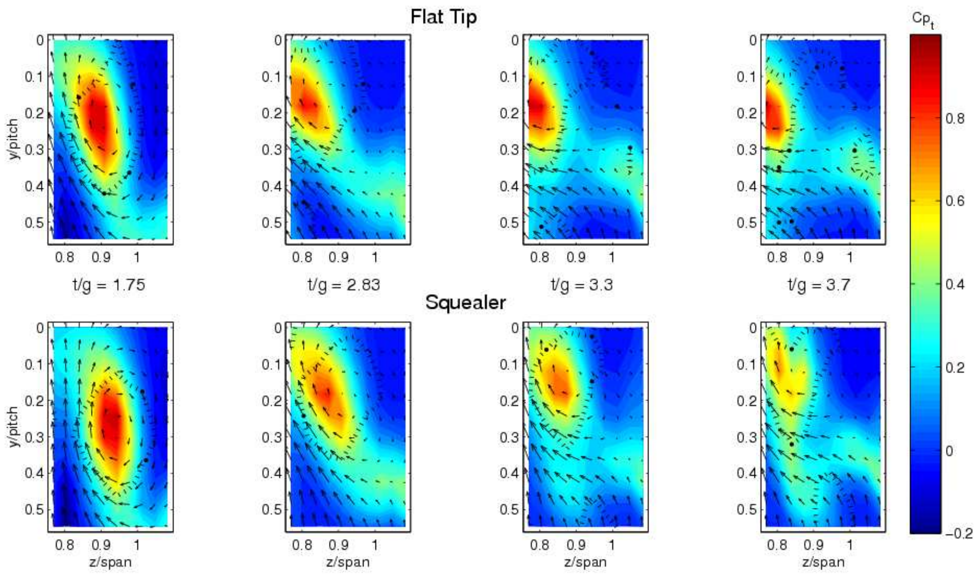

Figure 9. Coefficient of pressure distribution for different winglets producing different thickness-to-gap ratios for a 8% gap to chord ratio.

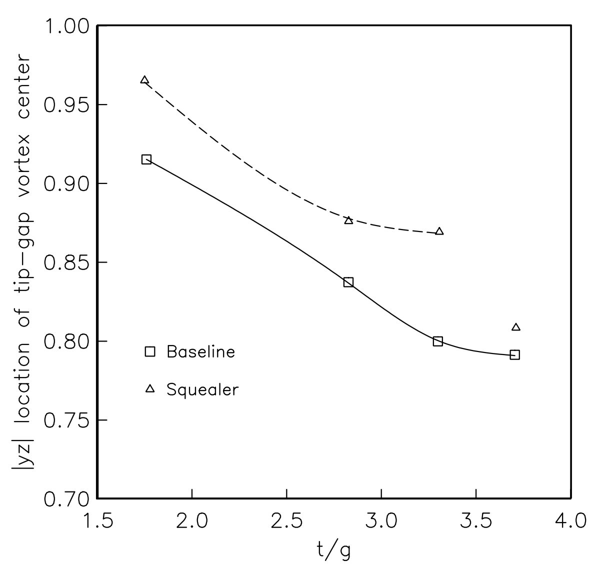

Figure 10. Magnitudes of the locations of the center of the tip-gap vortex as a function of the thickness-to-gap ratio at a 8% gap-to-chord ratio.

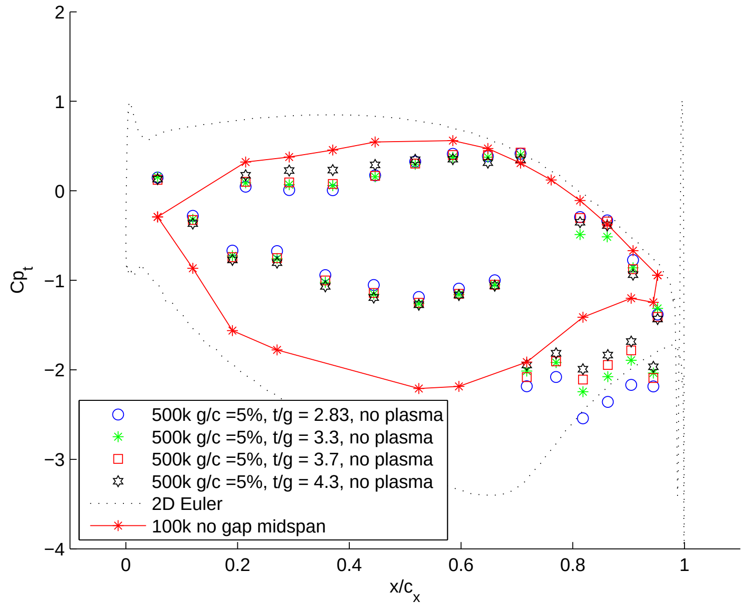

Figure 11. Pressure coefficient distribution at the end of the blade near the tip for a 5% gap-to-chord ratio and a range of thickness-to-gap ratios. Note no squealer installed.

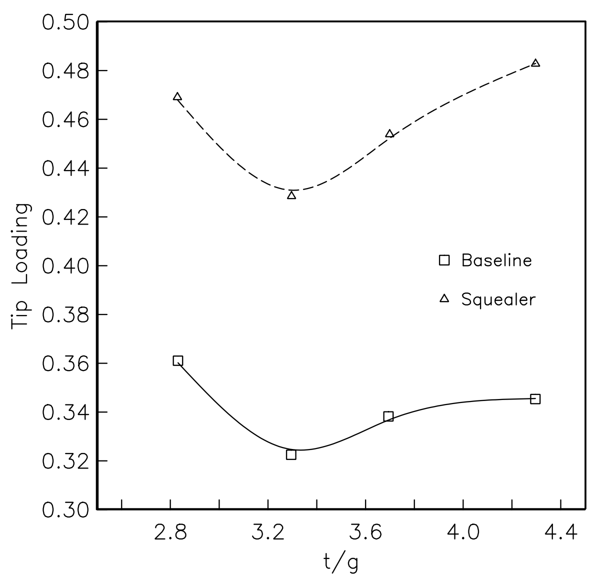

Figure 12. Blade loading as a function of thickness-to-gap ratio for a gap-to-chord ratio of 5%, with and without a squealer tip installed.

increase in the blade loading with increasing t/g. This apparently is a result of an increase in the strength of the tip-gap vortex as t/g increases. Note that most of the t/g values are within the "thin" blade regime.

The addition of the squealer tip reduces the blade loading at the lowest t/g, but subsequently increases the the blade loading at all the other larger t/g values. This points out the complexity of how the blade loading depends on a combination of the tip-gap blockage and the tip vortex strength.

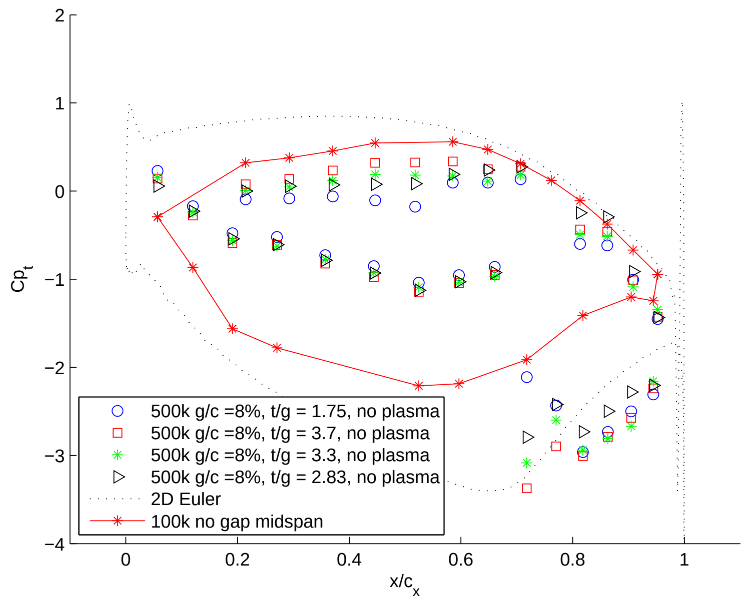

Figure 13. Pressure coefficient distribution at the end of the blade near the tip for a 8% gap-to-chord ratio and a range of thickness-to-gap ratios. Note no squealer installed.

More insight into the differences observed in the wake measurements and blade-tip loading was obtained from the surface flow visualization on the blade tips. These are shown for the 5% g/c in Figure 15, and for the 8% g/c in Figure 16. Recall that these surface visualization records consist of the tracks of ink dots that are assumed to follow the local shear stress on the end of blade that results from the flow through the gap. Three independent records were taken for each case, scanned digitally and averaged. Arrows have been added to provide an interpretation of the dot tracks.

Viewing the surface visualization records, there are a number of obvious features.

1. There is a well defined re-attachment line at which the shear direction bifurcates, with some vectors pointed towards the suction side, and others pointed towards the pressure side of the blade.

2. The arrows pointing towards the pressure side suggest a flow recirculation from the re-attachment point to the edge of the pressure side of the blade.

3. There is a well delineated portion of the blade at the leading edge at which the shear vectors indicate that the passage flow traverses through the gap without re-attaching on the blade.

Given these characteristic features of the surface visualization at the 5% and 8% g/c, the following can be concluded.

1. The region where the passage flow traverses through the gap without re-attaching on the blade moves further back along the chord of the blade as t/g increases.

2. The chordwise extent of the re-attachment line shortens as t/g increases.

3. The chordwise extent of the re-attachment line shortens as g/c increases, even for the same thickness-to-gap ratio.

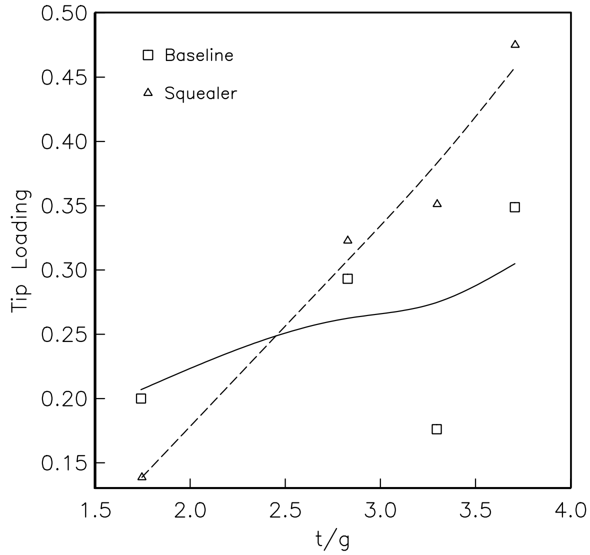

Figure 14. Blade loading as a function of thickness-to-gap ratio for a gap-to-chord ratio of 8%, with and without a squealer tip installed.

These results contradict Denton's proposal[7] that for "thin" blades the flow separates from pressure-side edge of the blade tip but never re-attaches. In fact, the opposite appears to be the case. To aid in illustrating this, the length of the region where the flow **does not re-attach** as a percentage of the blade chord is plotted in Figure 17. In both g/c cases, the extent where the flow does not re-attach increases linearly with t/g. This is opposite to the trend postulated by Denton.[7]

In addition with regards to the topology of the flow under the blade, there does not appear to be a sharp transition such as one would quantify as a "regime". Rather the change in topology appears to be relatively smoothly changing with t/g.

Aside from the designation of regimes, the existence and extent of the re-attachment line is important for active flow control because it represents a very receptive site for unsteady forcing. Since the re-attachment line was found to essentially extend to the trailing edge of the blade, its length corresponds to $1-(x/c_x)_{no-reattachment}$ in Figure 17. That length decreases as either t/g increases or g/c increases.

The surface flow visualization was also examined for the cases with the squealer tip. These are shown for the 5% g/c in Figures 18 and 19, and for the 8% g/c in Figures 20 and 21. Included with these are the surface flow visualization for the baseline cases that correspond to the squealer condition. Shown below the surface visualization are the corresponding wall pressure coefficient distributions. The color bar scales are the same for figures with the same g/c ratios. The location of the squealer is drawn on the surface visualization record as a thick black line.

The case with the 5% g/c for $t/g = 3.3$ is shown in Figure 18. The condition would nominally be in the "thin" blade region. As previously shown from the surface flow visualization for the baseline flat-tip blade, a region near the leading edge is observed in which the flow passes under the blade without re-attaching. Also observed is the bifurcation line for the vectors that we associated with the re-attachment of the separation bubble from the pressure-side edge of the blade. The corresponding pressure field is consistent with this interpretation. The flow in the gap-passage near the leading-edge of the blade appears as the highest positive C_p value. The region of the re-attachment line on the blade end appears as the largest negative (suction) pressure coefficients on the wall under the blade. The maximum suction pressure on the wall is at the trailing edge of the blade and probably reflects the effect of the tip-gap vortex.

The addition of the squealer tip has a dramatic effect on the flow under the blade as evidenced by the surface flow visualization and wall pressure distribution. The surface flow visualization indicates that a majority of the flow under the blade is turned, suggesting a large recirculation zone. The chordwise extent of this is comparable to the baseline case. The flow near the leading edge is turned by the squealer and vectored along the chord direction of the blade, feeding the recirculation zone. This large circulation formed by the squealer is a major drawback of this passive flow control because it would enhance heat transfer that could erode the blade tip.

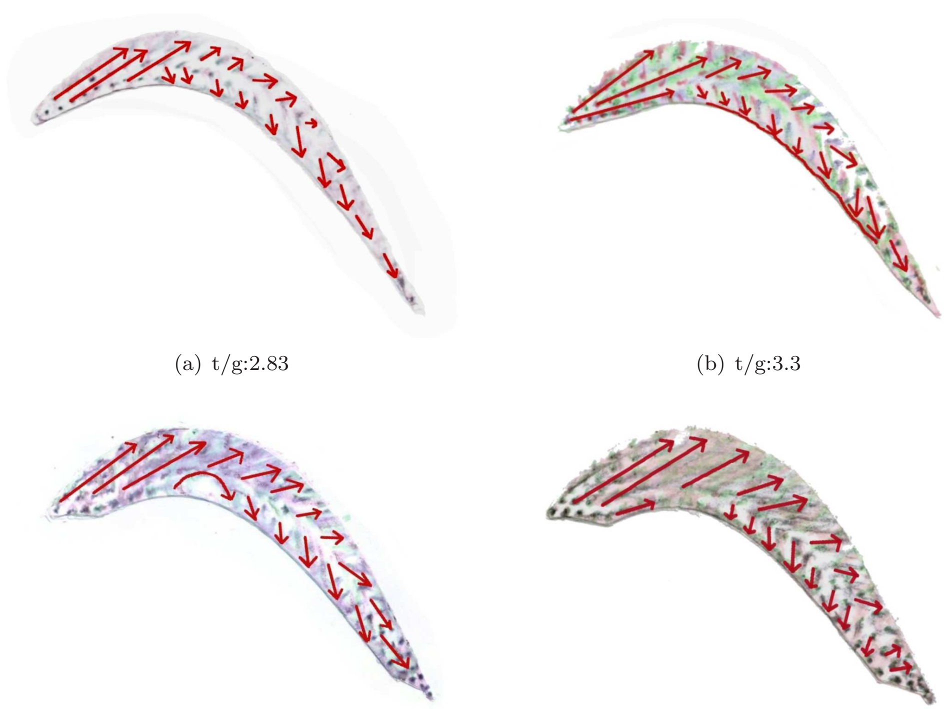

(a) t/g:2.83

(b) t/g:3.3

(c) t/g:3.7

(d) t/g:4.3

Figure 15. Surface flow visualization at the blade tip for a range of thickness-to-chord ratios at a gap-to-chord ratio of 5%. Note no squealer installed.

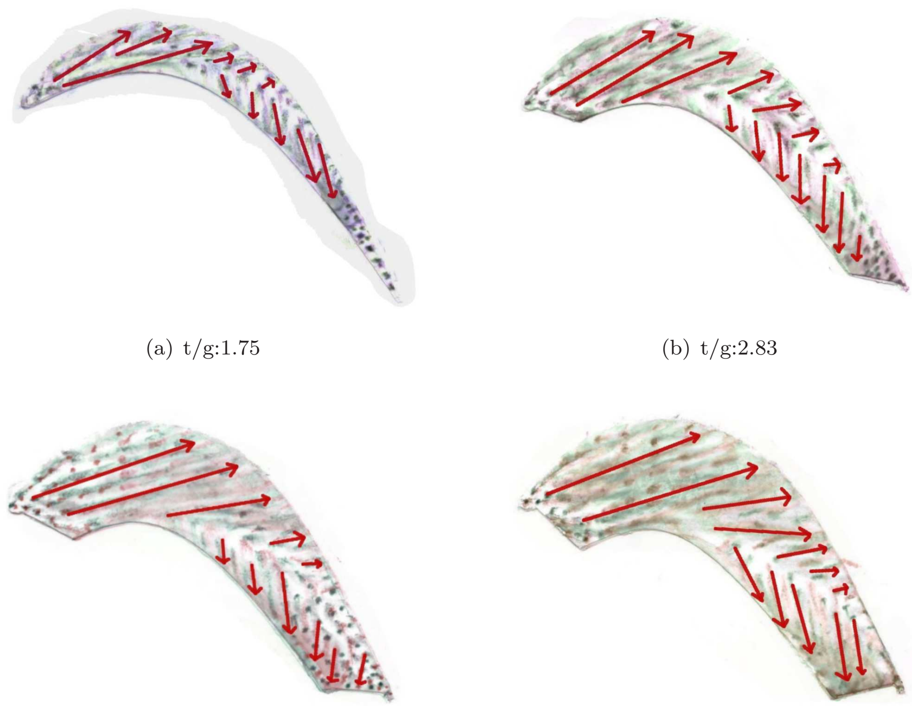

(a) t/g:1.75

(b) t/g:2.83

(c) t/g:3.3

(d) t/g:3.7

Figure 16. Surface flow visualization at the blade tip for a range of thickness-to-chord ratios at a gap-to-chord ratio of 8%. Note no squealer installed.

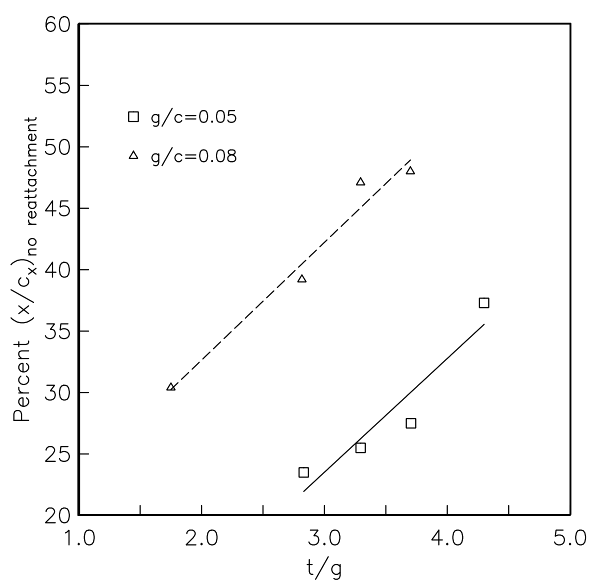

(a) $g/c = 5\%$

Figure 17. Length of region without re-attachment as a percentage of x-chord as a function of thickness-to-gap ratio for $g/c = 0.05$ and 0.08.

With regards to the wall pressure distribution, higher C_p values occur on the pressure side of the blade with the squealer tip. The suction pressure at the trailing edge in this case appears lower, possibly indicating a weakening of the tip-gap vortex. Overall however, the blade tip loading was higher as was shown in Figure 12.

The case with the 5% gap-to-chord for $t/g = 4.3$ is shown in Figure 18. This condition would nominally be in the "thick" blade regime. The corresponding pressure field is shown below the surface visualization. Overall the behavior is similar to the that at the smaller g/c.

The addition of the squealer tip again has a similar dramatic effect on the flow under the blade. For the base flow, the larger t/g results in a larger portion of the flow at the leading edge that would normally pass through the gap without attaching to the underside of the blade tip. This flow is captured by the squealer tip and vectored along the chord direction of the blade. This resulted in higher shear on the blade surface that was evidenced in the longer ink streaks. These changes are visible in the wall pressure distribution especially near the trailing edge where the C_p values are noticeably higher (less negative) than in the flat-tip case. This is consistent with the measured increase in the blade tip loading (Figure 12).

(a) flat tip (b) squealer

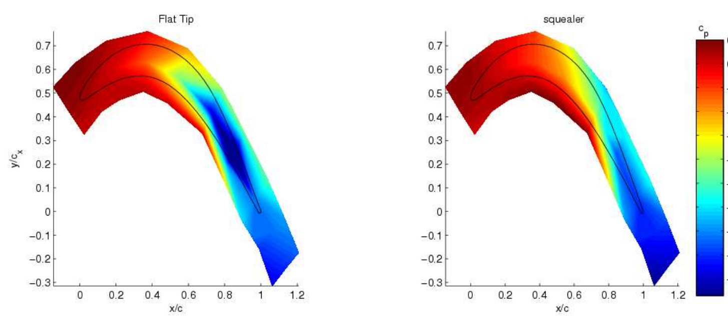

(c) endwall

Figure 18. Surface flow visualization at the blade tip and pressure coefficient readings on the endwall for a gap-to-chord ratio of 5% and a thickness-to-gap of 3.3 with and without squealer.

Figures 20 and 21 document the effect of the squealer tip on the surface flow visualization and wall pressure for the 8% g/c. Figure 20 corresponds to $t/g = 2.83$ which is nominally in the "thin" blade regime, and Figure 21 corresponds to $t/g = 3.7$ which is on the lower edge of the "thick" blade regime.

The surface visualization for the 8% g/c baseline cases show the further lengthening of the region near the leading edge in which the flow passes under the blade without re-attaching. For the smaller $t/g = 2.83$ case, the addition of the squealer tip redirects the flow near the tip as before. However one difference that is evident with the squealer tip on the larger g/c blade is a line of high shear that occurs close to and follows the edge of the pressure side of the downstream 60% of the blade. Whatever the significance of this, the wall pressure distribution indicated very little change with the addition of the squealer tip, and only a slight increase in the blade tip loading (Figure 14). Although the larger $t/g = 3.7$ at the 8% g/c, had shown more of a blade-tip loading increase with the squealer compared to the smaller t/g, there was not any significant change in the flow topology evident in the surface flow visualization or wall pressure distributions.

(a) flat tip (b) squealer

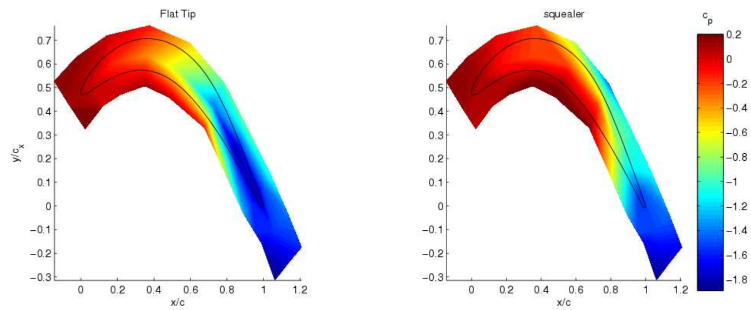

(c) endwall

Figure 19. Surface flow visualization at the blade tip and pressure coefficient readings on the endwall for a gap-to-chord ratio of 5% and a thickness-to-gap of 4.3 with and without squealer.

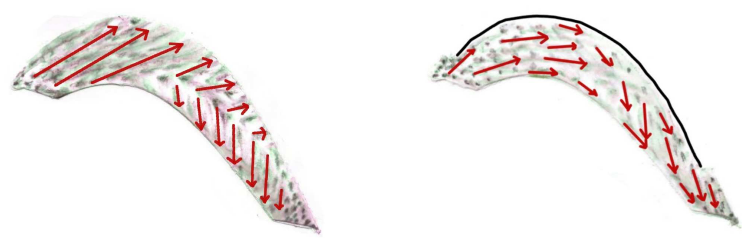

(a) flat tip (b) squealer

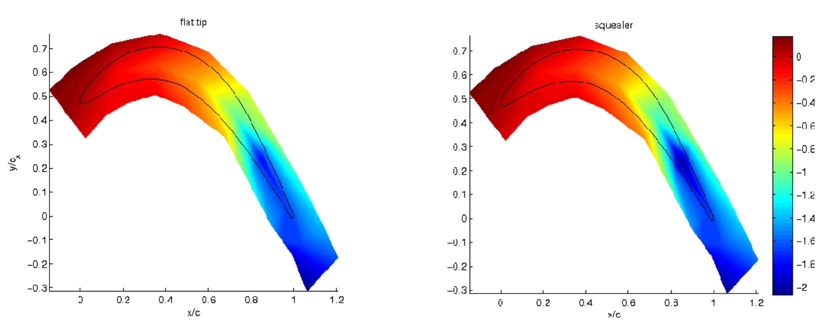

(c) endwall

Figure 20. Surface flow visualization at the blade tip and pressure coefficient readings on the endwall for a gap-to-chord ratio of 8% and a thickness-to-gap of 2.83 with and without squealer.

(a) flat tip

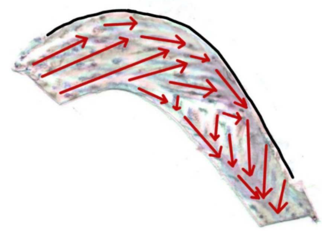

(b) squealer

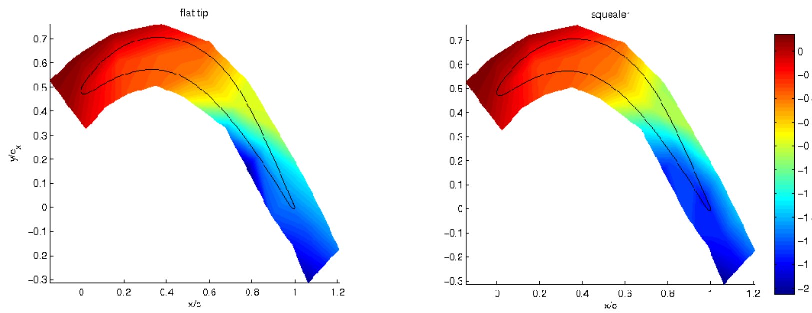

(c) endwall

Figure 21. Surface flow visualization at the blade tip and pressure coefficient readings on the endwall for a gap-to-chord ratio of 8% and a thickness-to-gap of 3.7 with and without squealer.

IV. Conclusion

An experiment was conducted in a linear cascade of Pak-B blades for an exit Mach number of 0.3 to simulate the flow in the tip gap region of a low pressure turbine blade row. The experiment focused on the independent effects of thickness-to-gap and gap-to-chord ratios on the flow behavior. Two extreme gap-to-chord ratios of 5% and 8% were chosen, for which four thickness-to-gap ratios were examined. The flow was documented through blade-tip and end-wall static pressure measurements, and downstream total pressure loss coefficients. Additionally, surface flow visualization was performed on the blade tip end for a greater understanding of the gap-flow behavior. The response of the flow to passive flow control using a partial suction-side squealer tip at each of the thickness-to-gap and gap-to-chord cases was documented. The intention was to examine any sensitivity of the flow to the gap-to-chord ratio that might be attributed to the thickness-to-gap ratio in a manner that can be categorized as “thick” and “thin” blade behavior. For this, the focus was on possible changes in the size and location of a separation and re-attachment line on the blade tip end.

The results presented in this paper indicate that the behavior of the flow in the tip gap region of a linear cascade turbine blade depend **both** on thickness-to-gap and the gap-to-chord ratios. In all cases regardless of the thickness-to-gap, the surface flow visualization revealed a well defined re-attachment line at which the shear direction bifurcates, with some vectors pointed towards the suction side, and others pointed towards the pressure side of the blade. This re-attachment was associated with the flow separation from the pressure-side edge of the blade tip. The re-attachment line never reached to the leading edge of the blade. Rather there was a well delineated portion of the blade at the leading edge at which the shear vectors indicate that the passage flow traversed through the gap without re-attaching.

Given these characteristic features of the surface visualization, as the thickness-to-gap ratio increased, the region where the passage flow traverses through the gap without re-attaching moves further back along the chord of the blade. Commensurate with this was a decrease in the chordwise extent of the re-attachment line. The chordwise extent of the re-attachment line also shortened as the gap-to-chord increased, even for the same thickness-to-gap ratio. This contradicts previous suggestions that “thin” blade behavior lacks a flow re-attachment in the tip-gap region of the blade.

Even though a "thin/thick" regime could not be correlated with the presence or lack of a separation/re-attachment line on the blade end, there was evidence in other features of the tip-gap flow of "thin" and "thick" blade behavour. This appeared in the location from the wall of the maximum loss coefficient associated with the tip-gap vortex, and with the blade-tip loading. Based on these, the boundary between the two regimes is at $t/g \simeq 3.5$, which also agrees with the observations of Douville et al.[15]

The effect of squealer tips was found to primarily depend on the gap-to-chord ratio. At a 5% g/c, the squealer tip increased the blade tip loading for the full range of the thickness-to-gap ratios, encompassing "thin" and "thick" regimes. The surface flow visualization indicated that a majority of the flow under the blade was turned by the squealer tip, suggesting a large recirculation zone. The chordwise extent of this was comparable to the baseline case. The flow near the leading edge was turned and vectored along the chord direction of the blade, feeding the recirculation zone. This large circulation formed by the squealer is a major drawback of this passive flow control because it could enhance heat transfer that could erode the blade tip. At the higher 8% g/c, the squealer tip had only a small improvement on the blade tip loading at a smaller t/g that fell within the "thin" regime, but a somewhat larger improvement for the larger t/g that fell in the lower edge of the "thick regime".

Finally, defining the locations of the separation and re-attachment lines is important to our goals of active tip-gap flow control using plasma actuators because such flow features are traditionally highly receptivity to unsteady forcing. The ultimate intention is to affect the tip-vortex formation and downstream mixing by exciting an instability of the blade-gap flow by unsteady forcing through a plasma actuator located on the blade tip.

Acknowledgement

The authors would like to thank the Air Force Office of Scientific Research (Grant No. FA9550-04-1-0198) for supporting this work.

References

[1]Lattime, S. B. and Steinetz, B. M., "Turbine Engine Clearance Control Systems: Current Practices and Future Directions," Nasa/tm–2002-211794, Ohio Aerospace Institute, Brook Park, Ohio, 2002.

[2]Yamamoto, A., "Production and Developement of Secondary Flows and Losses Within Two Types of Straight Turbine Cascades: Part 1–A Stator Case," *ASME Journal of Turbomachinery*, Vol. 109, 1987, pp. 186–193.

[3]Yamamoto, A., "Production and Developement of Secondary Flows and Losses Within Two Types of Straight Turbine Cascades: Part 2–A Rotor Case," *ASME Journal of Turbomachinery*, Vol. 109, 1987, pp. 194–200.

[4]Sjolander, S. A. and Amrud, K. K., "Effects of Tip Clearance on Bleade Loading in a Planar Cascade of Turbine Blades," *ASME Journal of Turbomachinery*, Vol. 109, 1987, pp. 237–245.

[5]Yamamoto, A., "Endwall Flow/Loss Mechanisms in a Linear Turbine Cascade With Blade Tip Clearance," *ASME Journal of Turbomachinery*, Vol. 111, 1989, pp. 264–275.

[6]Bindon, J. P., "The Measurement and Formation of Tip Clearance Loss," *ASME Journal of Turbomachinery*, Vol. 111, 1989, pp. 257–263.

[7]Denton, J. D., "Loss Mechanisms in Turbomachines," *ASME Journal of Turbomachinery*, Vol. 115, 1993, pp. 621–651.

[8]Sjolander, S. A., "Physics of Tip-Clearnace Flows-i," *VKI Lecture Series*, Vol. 01, 1997, pp. 1–32.

[9]McCarter, A. A., *Investigation of Tip Clearance Flow Fields In A Turbine Rotor Passage*, Master's thesis, The Pennsylvania State University, University Park, PA, May 2000.

[10]A. A. McCarter, X. Xiao, B. L., "Tip Clearance Effects in a Turbine Rotor: Part II - Velocity Field and Flow Physics," *ASME Journal of Turbomachinery*, Vol. 123, 2001, pp. 305–313.

[11]T. C. Booth, P. R. D. and Hepworth, H. K., "Rotor-Tip Leakage: Part I–Basic Methodology," *ASME Journal of Turbomachinery*, Vol. 104, 1982, pp. 154–159.

[12]Key, N. L. and Arts, T., "Comparison of Turbine Tip Leakage Flow For Flat Tip and Squealer Tip Geometries at High-speed Conditions," *Proceedings of ASME Turbo Expo*, ASME, Vienna, Austria, 2004.

[13]M. Papa, R. J. Goldstein, F. G., "Effects of Tip Geometry and Tip Clearance On the Mass/Heat Transfer From a Large-Scale Gas Turbine Blade," *Proceedings from the ASME Turbo Exp*, ASME, Amsterdam, The Netherlands, 2002.

[14]F. G. Heyes, H. P. H. and Dailey, G. M., "The Effect of Blade Tip Geometry on the Tip Leakage Flow in Axial Turbine Cascades," *ASME Journal of Turbomachinery*, Vol. 114, 1992, pp. 643–651.

[15]T. Douville, J. Stephens, T. C. and Morris, S., "Turbine Blade Tip Leakage Flow Control by Partial Squealer Tip and Plasma Actuators," *Proceedings of 44th Aerospace Sciences Meeting*, AIAA, Reno, Nevada, 2006.

[16]Langston, L. S. and Boyle, M. T., "A New Surface-Streamline Flow Visualization Technique," *Journal of Fluid Mechanics*, Vol. 125, 1982, pp. 53–57.

[17]N. V. Aunapu, R. J. V. and Flack, K. A., "Surface Flow Visualization of a Scaled-Up Turbine Blade Passage," *Measurements in Science and Technology*, Vol. 11, 2000, pp. 987–991.